

1 **Lead and slant on the geometry of coiling in gastropods**

2

3 Ido Filin ¹ *

4 ¹ Independent researcher.

5 * Corresponding author. E-mail: ido@filin.fi

6

7 Running headline: Geometry of coiling.

8 Supplementary material: SI appendix.

9 The author(s) declare(s) no conflict of interest.

10 This manuscript was compiled on 15 May 2026.

11 **Abstract**

12 Molluscan shells have been studied with various geometric models. Here I show that
13 *lead angle*, the defining slope of a conical helix, emerges as a more useful parameter in
14 morphometric analyses and (adaptationist) interpretation of covariation in coiling parameters.
15 The widely used apical semiangle becomes redundant and uninformative, a passive
16 consequence of taxon-specific lead angles and plasticity in growth (expansion rate). Treating
17 coiled shells as conical helices, and extending to *logarithmic slant helices* (curves of
18 precession), provides insights into ontogenetic allometry, irregular coiling, past models, and
19 unifying fixed- and moving-frame approaches.

20

21 **Keywords:** allometry, conchology, developmental plasticity, logarithmic spiral,
22 ontogeny, slant helix, theoretical morphology

23 **Note**

24 The equiangular, or logarithmic, spiral has a long and distinguished history, going back to
25 Descartes, Torricelli, Christopher Wren, Newton, Halley, and the Bernoullis (Thompson [1942]
26 1992; Archibald 1918; Hammer 2016). Its application in biology, however, only picked up with
27 Canon (Henry) Moseley and Carl Friedrich Naumann around 1840, who applied it to the study
28 of molluscan shells, coinciding with the rapid development of paleontology in the 19th century
29 (Moseley 1838, 1842; Naumann 1845; Thompson [1942] 1992; Raup 1966; Vinarski 2014).
30 Much of this earlier work on modeling and measurement of shells is thoroughly and
31 eloquently summarized in D'Arcy Thompson's *magnum opus* "On Growth and Form"
32 (Thompson [1942] 1992).

33 In "The geometry of coiling in gastropods", Raup (1961) sketched an earlier version of his
34 parameter set for coiled geometries, that would later develop into theoretical morphology and
35 the morphospace concept (Raup & Michelson 1965; Raup 1966, 1967; McGhee 1999; Pappas &
36 Miller 2013; Gerber 2017). Essentially, though, Raup's model is a reformulation of the original
37 *conispiral* parametrization of Moseley (1838) and Thompson ([1942] 1992) – a logarithmic
38 spiral wrapped around a cone of *apical semiangle*, β , rather than winding on a plane
39 (planispiral coiling, $\beta \rightarrow \pi/2$; Fig. 1A,D). Its defining feature is a fixed *spiral angle*, α , between
40 the tangent of the spiral and its pole (or apex of the cone; hence, equiangular; Fig. 1A).

41 Conical logspirals also arise from fixed standardized *curvature* and *torsion* in the *differential*
42 *geometric* formulation of Okamoto (1988), a local (moving) frame analysis (Fig. 1B) that he
43 named the 'growing tube' model. A third alternative parameterization views the conical
44 logspiral as a *conical helix* (Fig. 1C). The defining feature of a helix (more accurately, general or
45 generalized helix, or curve of constant slope; Nutbourne & Martin 1988; Scofield 1995; SI) is
46 the constant angle its tangent makes with some fixed direction. This direction determines the
47 coiling axis, and the constant slope will be measured in this study by the downward angle of
48 the coil, or helical thread, termed *lead angle*, λ in Fig. 1D. (Preserving here the distinction
49 between 'pitch' and 'lead', in the case of multi-thread helical structures, i.e., double or triple
50 helices, or multi-start screws; see SI for more on terminology). If the coils wrap around a cone
51 ($0 < \beta < \pi/2$), rather than a cylinder ($\beta \rightarrow 0$; the familiar circular helices of springs and
52 corkscrews), such a conical helix is also a logarithmic conispiral. I dub this third
53 parameterization *conihelical*. (Not to be confused with the helicocone [Cox 1960] – the
54 expanding tube itself, which usually coils around an axis to form the spiral shell.)

55 In the words of D'Arcy Thompson, "It seems a complicated affair; but it is only a pathway
56 winding at a steady slope up a conical hill ... a certain ensemble, or bunch, of these spiral
57 curves in space constitutes the self-similar surface of the shell" (Thompson [1942] 1992). In
58 this note, I explore how conical helices and their "steady slope", or lead angle, have
59 underappreciated implications to morphometrics, interpretations of covariation in coiling
60 parameters, and unifying *fixed-* and *moving-frame* approaches to theoretical morphology. In
61 addition, conical helices can be extended to *slant helices*, particularly the *logarithmic slant*
62 *helix* that I present here, to gain better understanding of ontogenetic allometry, irregular
63 coiling, and previously formulated models of allometric spiral shells.

64 As hinted in the above quote, a shell is not a single conspiral, but a three-dimensional
65 structure made of "a bunch" of such spirals – the *multispiral* approach (Fig. 1E; also called
66 multivector; Thompson [1942] 1992; Bayer 1978; McGhee 1978, 1999; Savazzi 1990).
67 Alternatively, a shell can be described by a *generating curve*, a closed figure that sweeps
68 through space along a spiral *centerline* (Fig. 1F; Thompson [1942] 1992; Raup 1961, 1966;
69 Okamoto 1988; roughly corresponding to the 'aperture trajectory' of Stone 1995,
70 'curve-skeleton' of Monnet et al. 2009, 'ontogeny axis' of Liew & Schilthuizen 2016, or 'internal
71 spiral' of Larsson et al. 2020).

72 In self-similar isometrically growing conihelical shells, the different spirals that make the
73 shell's surface, by geometric necessity, differ in spiral angle, α , apical semiangle, β , and lead
74 angle, λ (Fig. 1E). However, they all share a single common value of exponential *expansion*
75 *rate*, γ , with respect to revolution angle, θ (Illert 1983). Given linear measures of shell size,
76 such as aperture size, a and b (Fig. 1F), centerline radius and height, r and z (Fig. 1D), or
77 centerline *arclength*, s , measured from the pole (or conical apex), one can define separate
78 expansion parameters for each. However, for self-similar conihelical shells, these expansion
79 rates are all equal, $\gamma_s = \gamma_a = \gamma_b = \gamma_z = \gamma_r = \gamma$. Alternatively, growth and size can be measured w.r.t
80 arclength, s , rather than revolution angle, θ . For example, the relations $a(s)$ and $b(s)$, for
81 aperture size, introduce Ackerly's (1989a) *dilation* parameter, which I denote here by
82 $q_a = da/ds$ and $q_b = db/ds$. In isometric conihelical shells, q_a and q_b are constants,
83 representing the opening angles of the expanding 'trumpet' or (helico)cone (Ekaratne & Crisp
84 1983; Ackerly 1989a; Vermeij 1993, 2002) that is coiled upon itself to make the spiral shell.
85 Dilation factors for centerline r and z are just $q_r = \cos \alpha \sin \beta$ and $q_z = \sin \lambda = \cos \alpha \cos \beta$.

86 A set of formulas relates the conspiral, conihelical, and differential geometric
87 parameterizations to each other and to expansion rates. One such formula is the

88 aforementioned expression for q_z , relating lead angle, λ , to spiral angle, α . For expansion rate,

89
$$\cot \alpha \sin \beta = \gamma \tag{1}$$

90 (Moseley 1842; Thompson [1942] 1992; Raup & Graus 1972; Løvtrup & von Sydow 1974;
91 Ekaratne & Crisp 1983; Illert 1983). Gastropod shells usually exhibit several complete whorls.
92 Consequently, expansion rate is typically small, $\gamma \leq 0.2$ (Thompson [1942] 1992; Cameron
93 1981), leading to a similar, approximate, expression for the conihelical parameterization,

94
$$\tan \lambda \tan \beta \approx \gamma \tag{2}$$

95 (the exact expression being $\tan \lambda \tan \beta = \gamma / \sqrt{1 + \gamma^2}$; see SI for discussion of approximation
96 errors), demonstrating the three-way covariation of expansion rate, apical semiangle and lead
97 angle.

98 Many empirical studies of shell coiling, in the past 50 years, have provided estimates of
99 Raup's T and W parameters; or in terms of this study, $\tan \beta = 1/T$ and $\gamma = \ln W / 2\pi$ respectively.
100 Covariation of $\tan \beta$ and γ may point to adaptation, such as for mechanical strength, postural
101 stability or economical shell construction (Raup 1966; Noshita et al. 2012; Okabe & Yoshimura
102 2017; Páll-Gergely et al. 2024), and is usually interpreted through Raup's (1966) condition for
103 tight coiling, or whorl overlap, $\tan \beta > \sinh(\pi\gamma)$, given circular apertures (SI). (Alternatively,
104 $\sin \beta > \tanh(\pi\gamma)$; corresponding to the expression by Clarke et al. 1999, accounting for the typo
105 in their equation, and the difference in definition of apical angle; SI). However, for small γ ,
106 typical of most gastropods, the whorl overlap boundary is practically indistinguishable from
107 the seemingly arbitrary condition $\lambda < \arctan(1/\pi)$ (0.318 or 17.66° ; Fig. 2A; SI). Similar
108 conditions can be formulated for non-circular apertures (SI). A geometric constraint on lead
109 (or spiral) angle, combined with variation in growth rate (shell expansion), can therefore
110 produce, given Eq.[2], the empirically observed direct relation between $\tan \beta$ and γ .

111 Past hints to the relative constancy of lead angles can also be glimpsed from observations
112 of ontogenetic patterns, where measurements of $\tan \beta$ and γ at different whorls or
113 developmental stages vary together, so to preserve an almost fixed ratio (e.g., Newkirk & Doyle
114 1975; Hutchinson 1989; Clarke et al. 1999). In particular, Ekaratne & Crisp's (1983)
115 shell-height-to-arclength ratio contains a $1/\sec \alpha \sec \beta$ factor, which is just $q_z = \sin \lambda$ of this
116 study. In fact, their formula can be rewritten as $H/s = z/s + b/s = q_z + q_b = \sin \lambda + q_b$ (SI).
117 Lead angle, therefore, a defining feature of conical helices, emerges as a more useful
118 parameter for interpreting morphometric (co)variation (Fig. 2B). Variation in apical semiangle

119 (β ; Fig. 2A) follows as a passive consequence of growth (variation in γ) and geometry (lead
120 angle, λ) of the expanding centerline spiral (Eq.[2]).

121 Lead angle, however, is expected to vary ontogenetically to some degree. For example,
122 Savazzi (1990) discussed deviated protoconchs (see also Cox 1960; Shuto 1974; Frýda &
123 Ferrová 2011); van Osselaer & Grosjean (2000) fitted conispirals piecewise to several species,
124 and showed three ontogenetic phases – protoconch, and early and late conispiral phases –
125 with different coiling parameters (see also Davoli & Russo 1974); and Newkirk & Doyle (1975)
126 reported values of coiling parameters for embryos and adults in a study of geographic
127 variation in the rough periwinkle, *Littorina saxatilis* (Fig. 2).

128 Variation in lead angle can be further understood by considering the differential geometric
129 parameterization. In helices, coiling angle per unit of centerline arclength, $d\theta/ds$, is measured
130 by the norm of the Darboux vector, $\mathbf{u} = u\hat{\mathbf{u}}$, the rotation vector of the Frenet frame along its
131 defining space curve (Fig. 1B; Chouaieb et al. 2006; Goriely 2017). In generalized helices, $\hat{\mathbf{u}}$
132 coincides with the fixed coiling axis. The norm of the Darboux vector, $\|\mathbf{u}\| = u$, is the
133 ‘compound curvature’ of Nutbourne & Martin (1988), the ‘first alternative curvature’ of
134 Güzelkardeşler & Şahiner (2024), and the familiar $\sqrt{\kappa^2 + \tau^2}$ of differential geometric literature
135 (also D_G and A_G of Noshita 2014 and Noshita et al. 2016, who used Okamoto’s growing tube
136 formulation; clearly related in their expressions to angular rate, $d\theta/ds$). In this note, I refer to u
137 as *local coiling*. The constant lead angle of general helices is determined by the
138 torsion-curvature ratio, $\tan \lambda = \tau/\kappa$, $\kappa = u \cos \lambda$, and $\tau = u \sin \lambda$.

139 Conical helices are further defined by local coiling that is inversely proportional to arclength,
140 s (Nutbourne & Martin 1988). We can, therefore, write $u = \tilde{u}/s$, where \tilde{u} is constant
141 dimensionless *standardized local coiling* (though the ‘standardization’ here is different than
142 Okamoto’s). Arclength expansion rate, γ_s , is then related to (standardized) local coiling by the
143 simple and intuitive relation $\gamma_s = 1/\tilde{u}$ (SI). As local coiling and curvature increase, the conical
144 helix coils tighter, and less arclength growth and radial expansion is gained per full revolution.
145 Hence, more whorls are required for a specified amount of (relative) growth. This helps to
146 explain the association of high-spired species with large numbers of whorls (Cain 1980) and
147 Gould’s so-called “jigsaw constraint”, originally observed in his study of *Cerion* (Gould 1989;
148 Béguinot 2021).

149 Allometric modifications of conical helices, such as the logarithmic *helicospiral* model,
150 derived many times in various guises (essentially, $\gamma_z \neq \gamma_r$; Kohn & Riggs 1975; Bayer 1978;
151 Cortie 1989; Schindel 1990; Savazzi 1990; Fowler et al. 1992; Stone 1995; Tursch 1997;

152 van Osselaer & Grosjean 2000; Urdy et al. 2010; Swan 2015; Larsson et al. 2020), and Harary &
 153 Tal's (2011) 'natural 3D spiral', do not have constant lead angles, and therefore, are not
 154 generalized helices. Rate of change in lead angle, $\lambda' = d\lambda/ds$, is equivalent to the 'second
 155 alternative curvature' of Uzunoğlu et al. (2016) and Güzelkardeşler & Şahiner (2024) (see SI). If
 156 $\lambda' \neq 0$, the Darboux vector of local coiling and the fixed coiling axis of the helicospiral do not
 157 coincide, as the former now rotates around the latter (Fig. 1G). This new rotation axis is

$$\begin{aligned} \mathbf{w} &= w\hat{\mathbf{w}} = \mathbf{u} + \lambda'\hat{\mathbf{n}} = u\hat{\mathbf{u}} + \lambda'\hat{\mathbf{n}}, \\ w &= \|\mathbf{w}\| = \sqrt{u^2 + (\lambda')^2} = \sqrt{\kappa^2 + \tau^2 + (\lambda')^2}, \end{aligned} \quad (3)$$

159 dubbed here respectively vector and rate of *total coiling*. This full coiling rate (and direction)
 160 contains both a local coiling component, u , and a λ' component (first and second 'alternative
 161 curvatures' of Uzunoğlu et al. 2016 and Güzelkardeşler & Şahiner 2024; generalized helices are
 162 obtained when $\lambda' = 0$). The latter can be referred to as *coiling precession* rate, further explained
 163 at the end of this note.

164 Four decades ago, Løvtrup & Løvtrup (1988) attempted to "move the β parameter down to
 165 the mantle edge". In other words, derive a parameter of global shell shape from local
 166 processes occurring at the aperture. Løvtrup & Løvtrup's partial solution was to replace β with
 167 the ratio of maximum and minimum growth rates around the aperture. An explanation that
 168 Hutchinson (1990) debunked shortly after. Through Eqs.[1] and [2], however, the apical
 169 semiangle can indeed be "eliminated", or "moved down" to the aperture, as γ , α , and λ are
 170 defined at the growing tip (i.e., tangent) of conispirals, or conical helices. The distinction
 171 between fixed- (conispiral and conihelical) and moving-frame (differential geometric)
 172 parameterizations, thus, begins to blur.

173 Another defining feature of fixed-frame models is, for obvious reasons, the fixed coiling
 174 axis. Rate of change in the direction of local coiling, $\hat{\mathbf{u}}$, is given by $\hat{\mathbf{u}}' = \mathbf{w} \times \hat{\mathbf{u}} =$
 175 $u\hat{\mathbf{u}} \times \hat{\mathbf{u}} + \lambda'\hat{\mathbf{n}} \times \hat{\mathbf{u}} = \lambda'\hat{\mathbf{n}} \times \hat{\mathbf{u}}$. In conihelical shells ($\lambda' = 0$), the Darboux vector, \mathbf{u} , defines the fixed
 176 coiling axis. Thus, given starting coiling direction (initial condition), conispiral coiling can be
 177 defined by apical and spiral angles, by lead angle and expansion rate, by lead angle and
 178 standardized local coiling, \tilde{u} , or by Okamoto's standardized curvature and torsion. In all four
 179 cases, if parameter values remain fixed, the initial coiling direction is maintained ($\hat{\mathbf{u}}' = 0$),
 180 becoming a fixed axis, and self-similar conispiral shells result. That is another metric by which
 181 the distinction between fixed- and moving-frame parametrizations seems superfluous.

182 Irregular coiling, allometry, or other deviations from self-similar conihelical geometry,
 183 always require a change in parameter values (notably, lead angle). Gradual rotation of the

184 local coiling axis, $\hat{\mathbf{u}}$, thus, occurs simultaneously with (transient) change in lead angle ($\lambda' \neq 0$),
 185 and by rotating around the vector of total coiling, \mathbf{w} (Fig. 1G). That is, in fact, another direct
 186 consequence of conihelical geometry; this time, prescribing a testable hypothesis on how
 187 shell geometry can deviate from isometric conihelical. Some evidence in support of this
 188 hypothesis appears in Ackerly's (1989b) visual and stereographic analyses of *Vermicularia*,
 189 which possesses a tightly coiled conspiral juvenile phase, followed by an open-coiled
 190 geometry that differs in both coiling axis and lead angle. Similarly, his analysis of *Distorsio*
 191 shows that lead angle varies among successive episodic growth increments, while the
 192 per-increment coiling axis wobbles with an angular radius of roughly four to seven degrees.
 193 Savazzi (1996) provides examples from several species of *Tenagodus* (syn. *Siliquaria*) and
 194 *Vermicularia* that follow the same rule of simultaneous change in coiling axis and in lead
 195 angle. Particularly extreme cases occur in microsnails (Clements et al. 2008; Liew et al. 2014)
 196 and in irregularly coiled (heteromorph) ammonoids (Okamoto 1988, 1996).

197 Initially, the allometric logarithmic helicospiral ($\gamma_z \neq \gamma_r$) seems to contradict the hypothesis,
 198 as lead angle increases ($\gamma_z > \gamma_r$) or decreases ($\gamma_z < \gamma_r$), while the coiling axis remains fixed.
 199 Similarly, in Harary & Tal's (2011) 'natural 3D spiral', lead angle varies smoothly between a
 200 starting value, λ_0 , and an asymptotic value, λ_∞ , at large arclengths; essentially, converging to a
 201 conspiral (though adult size and shape may be obtained well before that asymptote is
 202 reached). However, when the direction of $\mathbf{w} = u\hat{\mathbf{u}} + \lambda'\hat{\mathbf{h}}$ does not change, it acts as the new
 203 fixed coiling axis of the shell; its magnitude, $w = \sqrt{u^2 + (\lambda')^2}$, is the coiling rate around that axis
 204 (i.e., revolution angle per unit growth of centerline arclength, $d\theta/ds = w = \|\mathbf{w}\|$). This rotation of
 205 the local moving Frenet frame around a potentially fixed axis, $\hat{\mathbf{w}}$, is another reason why fixed-
 206 and moving-frame models should be considered in tandem, as complementary points of view.

207 The condition of fixed $\hat{\mathbf{w}}$ is satisfied, for example, when local coiling and change in lead
 208 angle are both constant, $u = \text{const}$, $\lambda' = \text{const}$. These are the 'modulated curves' of Nutbourne &
 209 Martin (1988), better known as 'curves of constant precession' (Scofield 1995). Another class
 210 of curves, in which $\hat{\mathbf{w}}$ is fixed, are the already familiar conical and generalized helices. This is
 211 just the degenerate case of $\mathbf{w} = \mathbf{u}$ and $\lambda' = 0$, where the precession vanishes. Extrapolating
 212 from both curves of constant precession and curves of constant slope (generalized helices),
 213 one obtains a class of curves called *slant helices* that includes the former two as special
 214 cases. A necessary and sufficient condition for a slant helix, in the notation of this study, is
 215 $\lambda' \propto u$, or $\lambda' = \sigma u$ where $\sigma = \text{const}$ (Izumiya & Takeuchi 2004 ; SI).

216 We can proceed still one step further and define the *logarithmic slant helix*, $u, \lambda' \propto 1/s$, or

217 $u = \tilde{u}/s$ and $\lambda' = \sigma \tilde{u}/s$, where σ and \tilde{u} are constants (SI). While the logarithmic slant helix
 218 describes an allometrically growing shell, it does share some properties with the isometric
 219 conical helix. For example, revolution angle and arclength are similarly related through
 220 $\theta \propto \ln(s/s_0)$, and therefore arclength expands exponentially, $s = s_0 e^{\gamma_s \theta}$, where $\gamma_s = 1/\tilde{w}$,
 221 $\tilde{w} = \tilde{u}\sqrt{1+\sigma^2}$. Another feature of logarithmic slant helices is that lead angle grows linearly with
 222 θ . Successive whorls, separated by a full revolution around the coiling axis ($\Delta\theta = 2\pi$), are
 223 always tilted relative to each other by the same amount, $\Delta\lambda = 2\pi\lambda'/w = 2\pi\sigma/\sqrt{1+\sigma^2}$ (Fig. 1H).
 224 (This last result is roughly reminiscent of angular increments in Hutchinson's [1989]
 225 'road-holding' model.)

226 The logarithmic slant helix, thus, is a natural allometric extension of the isometric conical
 227 helix, in the sense that, instead of being fixed on the same initial value (λ_0) throughout
 228 ontogeny, lead angle grows linearly (i.e., $\lambda(\theta) = \lambda_0 + c\theta$; $c = \text{const}$). In that respect, it is the
 229 simplest case of centerline allometry, and provides insight into other allometric models
 230 (helicospirals, $\gamma_z \neq \gamma_r$, or Harary & Tal 2011). Lead angle cannot grow indefinitely, unless coiling
 231 becomes open and irregular. But real shells have a finite number of whorls, and therefore, the
 232 logarithmic slant helix, like its older cousin, the conical helix, is a useful approximation. In
 233 particular, given expressions for the centerline curve, $x(\theta)$, $y(\theta)$, and $z(\theta)$ (SI), one can simulate
 234 such shells graphically (Fig. 1H,I).

235 Finally, Illert (1983, 1989) envisioned the coiled shell as a spiral clock spring (see also,
 236 Savazzi 1995; McGhee 1999). In light of this note, rather than a clock spring, the coiled shell
 237 may be viewed as a precessing gyroscope, or spinning top. In the moving and rotating Frenet
 238 frame, the total coiling vector, \mathbf{w} , analogous to the spin of the gyroscope, precesses around
 239 the $\hat{\mathbf{n}}$ direction at a rate λ' ; resulting in an "interchange between curvature and torsion"
 240 (Nutbourne & Martin 1988), respectively the $\hat{\mathbf{b}}$ - and $\hat{\mathbf{t}}$ -components of \mathbf{w} . The constant σ
 241 determines the tilt angle, just as a precessing gyroscope is tilted relative to the horizontal
 242 plane, with the tilt determining the rate of precession (here, $\lambda' \propto \sigma$). With this sort of Kirchhoff
 243 kinetic analogy (Nizette & Goriely 1999), we gain yet another viewpoint whereby moving- and
 244 fixed-frame modeling are complementary.

245 **Supplementary information**

246 Additional derivations, explanations, methods, and discussion are in the supplementary
247 information document.

248 **DATA AND SOFTWARE AVAILABILITY.** All data and code are available at
249 <https://doi.org/10.5281/zenodo.19763621>, for the data analyses (Fig. 2), and at
250 <https://doi.org/10.5281/zenodo.19895626>, for the WebGL application of theoretical
251 morphology of coiled shells (Fig. 1).

252 **References**

- 253 Ackerly SC (1989a). Kinematics of accretionary shell growth, with examples from brachiopods and
254 molluscs. *Paleobiology* 15: 147–164. [10.1017/s0094837300009337](https://doi.org/10.1017/s0094837300009337).
- 255 Ackerly SC (1989b). Shell coiling in gastropods; analysis by stereographic projection. *PALAIOS* 4:
256 374–378. <https://doi.org/10.2307/3514561>.
- 257 Araki A, Noshita K (2023). Theoretical morphological analysis of differential morphospace
258 occupation patterns for terrestrial and aquatic gastropods. *Evolution* 77: 1864–1873.
259 <https://doi.org/10.1093/evolut/qpad110>.
- 260 Archibald RC (1918). The logarithmic spiral (undergraduate mathematics clubs, topics for club
261 programs). *American Mathematical Monthly* 25: 189–193.
- 262 Bayer U (1978). Morphogenetic programs, instabilities, and evolution — a theoretical study. *Neues*
263 *Jahrb Geol Paläont Abh* 156: 226–261. [10.1127/njgpa/156/1978/226](https://doi.org/10.1127/njgpa/156/1978/226).
- 264 Béguinot J (2021). Adult shell-size regulation in conspirally-coiled shells: evidence for a widespread
265 negative covariance between whorls growth-rate and the final number of whorls in land snails.
266 *Annual Research & Review in Biology* 36: 95–106.
267 <https://doi.org/10.9734/arrb/2021/v36i1030439>.
- 268 Cain AJ (1980). Whorl number, shape, and size of shell in some pulmonate faunas. *J Conchol* 30:
269 209–221.
- 270 Cameron RAD (1981). Functional aspects of shell geometry in some british land snails. *Biol J Linn Soc*
271 16: 157–167. <https://doi.org/10.1111/j.1095-8312.1981.tb01648.x>.
- 272 Chouaieb N, Goriely A, Maddocks JH (2006). Helices. *Proc Natl Acad Sci USA* 103: 9398–9403.
273 <https://doi.org/10.1073/pnas.0508370103>.
- 274 Clarke RK, Grahame J, Mill PJ (1999). Variation and constraint in the shells of two sibling species of
275 intertidal rough periwinkles (Gastropoda: *Littorina* spp.). *J Zool* 247: 145–154.

276 [10.1111/j.1469-7998.1999.tb00978.x](https://doi.org/10.1111/j.1469-7998.1999.tb00978.x).

277 Clements R, Liew TS, Vermeulen JJ, Schilthuizen M (2008). Further twists in gastropod shell
278 evolution. *Biology Letters* 4: 179 – 182. <https://doi.org/10.1098/rsbl.2007.0602>.

279 Cortie M (1989). Models for mollusc shell shape. *South African Journal of Science* 85: 454–460.

280 Cox LR (1960). Gastropoda. General characteristics of Gastropoda. In *Treatise on Invertebrate*
281 *Paleontology*, Part I, pp. I84–I169. Geological Society of America and University of Kansas Press,
282 New York, NY and Lawrence, KS.

283 Davoli F, Russo F (1974). Una metodologia paleontometrica basata sul modello di Raup: verifica
284 sperimentale su rappresentanti fossili del gen. *Subula* Schumacher. *Bollettino della Società*
285 *Paleontologica Italiana* 13: 108–121.
286 <https://www.paleoitalia.it/wp-content/uploads/2023/04/5-Davoli-Russo.pdf>.

287 Ekaratne SUK, Crisp DJ (1983). A geometric analysis of growth in gastropod shells, with particular
288 reference to turbinate forms. *Journal of Marine Biology Association UK* 63: 777–797.
289 [10.1017/S0025315400071216](https://doi.org/10.1017/S0025315400071216).

290 Fowler DR, Meinhardt H, Prusinkiewicz P (1992). Modeling seashells. *Proceedings of the 19th annual*
291 *conference on Computer graphics and interactive techniques*, pp. 379–387. [10.1145/133994.134096](https://doi.org/10.1145/133994.134096).

292 Frýda J, Ferrová L (2011). The oldest evidence of non-coaxial shell heterostrophy in the class
293 Gastropoda. *Bull Geosci* 86: 765–776. [10.3140/bull.geosci.1302](https://doi.org/10.3140/bull.geosci.1302).

294 Gerber S (2017). The geometry of morphospaces: lessons from the classic Raup shell coiling model.
295 *Biol Rev* 92: 1142–1155. <https://doi.org/10.1111/brv.12276>.

296 Goriely A (2017). *The Mathematics and Mechanics of Biological Growth*. Springer.
297 <https://doi.org/10.1007/978-0-387-87710-5>.

298 Gould SJ (1989). A developmental constraint in *Cerion*, with comments on the definition and
299 interpretation of constraint in evolution. *Evolution* 43: 516–539.
300 [10.1111/j.1558-5646.1989.tb04249.x](https://doi.org/10.1111/j.1558-5646.1989.tb04249.x).

301 Güzelkardeşler G, Şahiner B (2024). An alternative approach to find the position vector of a general
302 helix. *Celal Bayar University Journal of Science* 20: 54–60. [10.18466/cbayarfbe.1479066](https://doi.org/10.18466/cbayarfbe.1479066).

303 Hammer Ø (2016). *Perfect Shape: Spiral Stories*. Springer.

304 Harary G, Tal A (2011). The natural 3D spiral. *Computer Graphics Forum* 30: 237–246.
305 <https://doi.org/10.1111/j.1467-8659.2011.01855.x>.

306 Hutchinson JMC (1989). Control of gastropod shell shape: the role of the preceding whorl. *J Theor*

307 *Biol* 140: 431–444. [10.1016/S0022-5193\(89\)80107-9](https://doi.org/10.1016/S0022-5193(89)80107-9).

308 Hutchinson JMC (1990). Control of gastropod shell form via aperture growth rates. *J Morphol* 206:
309 259–264. [10.1002/jmor.1052060302](https://doi.org/10.1002/jmor.1052060302).

310 Illert C (1983). The mathematics of gnomonic seashells. *Math Biosci* 63: 21–56.
311 [10.1016/0025-5564\(83\)90049-4](https://doi.org/10.1016/0025-5564(83)90049-4).

312 Illert C (1989). Formulation and solution of the classical seashell problem. II. - Tubular
313 three-dimensional seashell surfaces. *Il Nuovo Cimento D* 11: 761–780. [10.1007/BF02451562](https://doi.org/10.1007/BF02451562).

314 Izumiya S, Takeuchi N (2004). New special curves and developable surfaces. *Turkish Journal of*
315 *Mathematics* 28: 153–164. [10.14943/83700](https://doi.org/10.14943/83700).

316 Kohn AJ, Riggs AC (1975). Morphometry of the *Conus* shell. *Syst Zool* 24: 346–359.
317 [10.1093/sysbio/24.3.346](https://doi.org/10.1093/sysbio/24.3.346).

318 Larsson J, Westram AM, Bengmark S, Lundh T, Butlin RK, Butlin RK (2020). A developmentally
319 descriptive method for quantifying shape in gastropod shells. *J R Soc Interface* 17.
320 <http://dx.doi.org/10.1098/rsif.2019.0721>.

321 Liew TS, Kok ACM, Schilthuizen M, Urduy S (2014). On growth and form of irregular coiled-shell of a
322 terrestrial snail: *Plectostoma concinnum* (Fulton, 1901) (Mollusca: Caenogastropoda:
323 Diplommatinidae). *PeerJ* 2: e383. <https://doi.org/10.7717/peerj.383>.

324 Liew TS, Schilthuizen M (2016). A method for quantifying, visualising, and analysing gastropod shell
325 form. *PLOS ONE* 11: 1–24. <https://doi.org/10.1371/journal.pone.0157069>.

326 Løvtrup S, Løvtrup M (1988). The morphogenesis of molluscan shells: a mathematical account using
327 biological parameters. *J Morphol* 197: 53–62. [10.1002/jmor.1051970105](https://doi.org/10.1002/jmor.1051970105).

328 Løvtrup S, von Sydow B (1974). D’Arcy Thompson’s theorem and the shape of the molluscan shell.
329 *Bull Math Biol* 36: 567–575. [10.1016/S0092-8240\(74\)80051-0](https://doi.org/10.1016/S0092-8240(74)80051-0).

330 McGhee GR (1978). Analysis of the shell torsion phenomenon in the Bivalvia. *Lethaia* 11: 315–329.
331 <https://doi.org/10.1111/j.1502-3931.1978.tb01889.x>.

332 McGhee GR (1999). *Theoretical Morphology: The Concept and Its Applications*. Perspectives in Earth
333 History and Paleobiology. Columbia University Press, New York.

334 Monnet C, Zollikofer C, Bucher H, Goudemand N (2009). Three-dimensional morphometric ontogeny
335 of mollusc shells by micro-computed tomography and geometric analysis. *Palaeontol Electron* 12:
336 1–13. <https://doi.org/10.5167/uzh-23587>.

337 Moseley H (1838). XVII. On the geometrical forms of turbinated and discoid shells. *Phil Trans R Soc*

338 128: 351–370. <https://doi.org/10.1098/rstl.1838.0018>.

339 Moseley H (1842). On conchylometry. *Lond Edinb Dubl Phil Mag* 21: 300–305.

340 <https://doi.org/10.1080/14786444208621551>.

341 Naumann CF (1845). Über die wahre Spirale der Ammoniten. *Annalen der Physik* 140: 538–543.

342 <https://doi.org/10.1002/andp.18451400406>.

343 Newkirk GF, Doyle RW (1975). Genetic analysis of shell-shape variation in *Littorina saxatilis* on an
344 environmental cline. *Mar Biol* 30: 227–237. [10.1007/BF00390745](https://doi.org/10.1007/BF00390745).

345 Nizette M, Goriely A (1999). Towards a classification of euler–kirchhoff filaments. *Journal of*
346 *Mathematical Physics* 40: 2830–2866. <https://doi.org/10.1063/1.532731>.

347 Noshita K (2014). Quantification and geometric analysis of coiling patterns in gastropod shells based
348 on 3D and 2D image data. *J Theor Biol* 363: 93–104. [10.1016/j.jtbi.2014.08.010](https://doi.org/10.1016/j.jtbi.2014.08.010).

349 Noshita K, Asami T, Ubukata T (2012). Functional constraints on coiling geometry and aperture
350 inclination in gastropods. *Paleobiology* 38: 322–334. [10.1666/10060.1](https://doi.org/10.1666/10060.1).

351 Noshita K, Shimizu K, Sasaki T (2016). Geometric analysis and estimation of the growth rate gradient
352 on gastropod shells. *J Theor Biol* 389: 11–19. [10.1016/j.jtbi.2015.10.011](https://doi.org/10.1016/j.jtbi.2015.10.011).

353 Nutbourne AW, Martin RR (1988). *Differential geometry applied to curve and surface design:*
354 *Foundations*. Ellis Horwood, Chichester, England.

355 Okabe T, Yoshimura J (2017). Optimal designs of mollusk shells from bivalves to snails. *Scientific*
356 *Reports* 7: 42445. <https://doi.org/10.1038/srep42445>.

357 Okamoto T (1988). Analysis of heteromorph ammonoids by differential geometry. *Paleobiology* 31:
358 35–52.

359 Okamoto T (1996). Theoretical modeling of ammonoid morphology. In *Ammonoid Paleobiology*
360 (edited by Landman NH, Tanabe K, Davis RA), pp. 225–251. Springer US, Boston, MA.

361 https://doi.org/10.1007/978-1-4757-9153-2_8.

362 Páll-Gergely B, Sipos AÁ, Harzhauser M, Örstan A, Winkler V, Neubauer TA (2024). Many roads to
363 success: alternative routes to building an economic shell in land snails. *Evolution* 78: 778–786.

364 <https://doi.org/10.1093/evolut/qpae018>.

365 Pappas JL, Miller DJ (2013). A generalized approach to the modeling and analysis of 3d surface
366 morphology in organisms. *PLOS ONE* 8: 1–15. <https://doi.org/10.1371/journal.pone.0077551>.

367 Raup DM (1961). The geometry of coiling in gastropods. *Proc Natl Acad Sci USA* 47: 602–609.

368 <https://doi.org/10.1073/pnas.47.4.602>.

369 Raup DM (1966). Geometric analysis of shell coiling: general problems. *J Paleontol* 40: 1178–1190.

370 Raup DM (1967). Geometric analysis of shell coiling: coiling in ammonoids. *J Paleontol* 41: 43–65.

371 Raup DM, Graus RR (1972). General equations for volume and surface area of a logarithmically coiled
372 shell. *Mathematical Geology* 4: 307–316. [10.1007/BF02114092](https://doi.org/10.1007/BF02114092).

373 Raup DM, Michelson A (1965). Theoretical morphology of the coiled shell. *Science* 147: 1294–1295.
374 [10.1126/science.147.3663.1294](https://doi.org/10.1126/science.147.3663.1294).

375 Savazzi E (1990). Biological aspects of theoretical shell morphology. *Lethaia* 23: 195–212.
376 [10.1111/j.1502-3931.1990.tb01360.x](https://doi.org/10.1111/j.1502-3931.1990.tb01360.x).

377 Savazzi E (1995). Theoretical shell morphology as a tool in constructional morphology. *Neues Jahrb*
378 *Geol Paläont Abh* 195: 229–240. [10.1127/njgpa/195/1995/229](https://doi.org/10.1127/njgpa/195/1995/229).

379 Savazzi E (1996). Adaptations of vermetid and siliquarid gastropods. *Palaeontology* 39: 157–177.

380 Schindel DE (1990). Unoccupied morphospace and the coiled geometry of gastropods: architectural
381 constraint or geometric covariation? In *Causes of Evolution: a paleontological perspective* (edited by
382 Ross R, Allmon W), pp. 270–304. University of Chicago Press, Chicago.

383 Scofield PD (1995). Curves of constant precession. *The American Mathematical Monthly* 102: 531–537.
384 <https://doi.org/10.1080/00029890.1995.12004613>.

385 Shuto T (1974). Larval ecology of prosobranch gastropods and its bearing on biogeography and
386 paleontology. *Lethaia* 7: 239–256. <https://doi.org/10.1111/j.1502-3931.1974.tb00899.x>.

387 Stone JR (1995). CerioShell: a computer program designed to simulate variation in shell form.
388 *Paleobiology* 21: 509–519. [10.1017/S0094837300013518](https://doi.org/10.1017/S0094837300013518).

389 Swan ARH (2015). Heterochrony in helicoid spiral cones: a computer model for demonstrating
390 heterochronic evolution. *Palaeontol Electron* 18: 1–11. [10.26879/510](https://doi.org/10.26879/510).

391 Thompson DW ([1942] 1992). *On Growth and Form: The Complete Revised Edition*. Dover, New York.

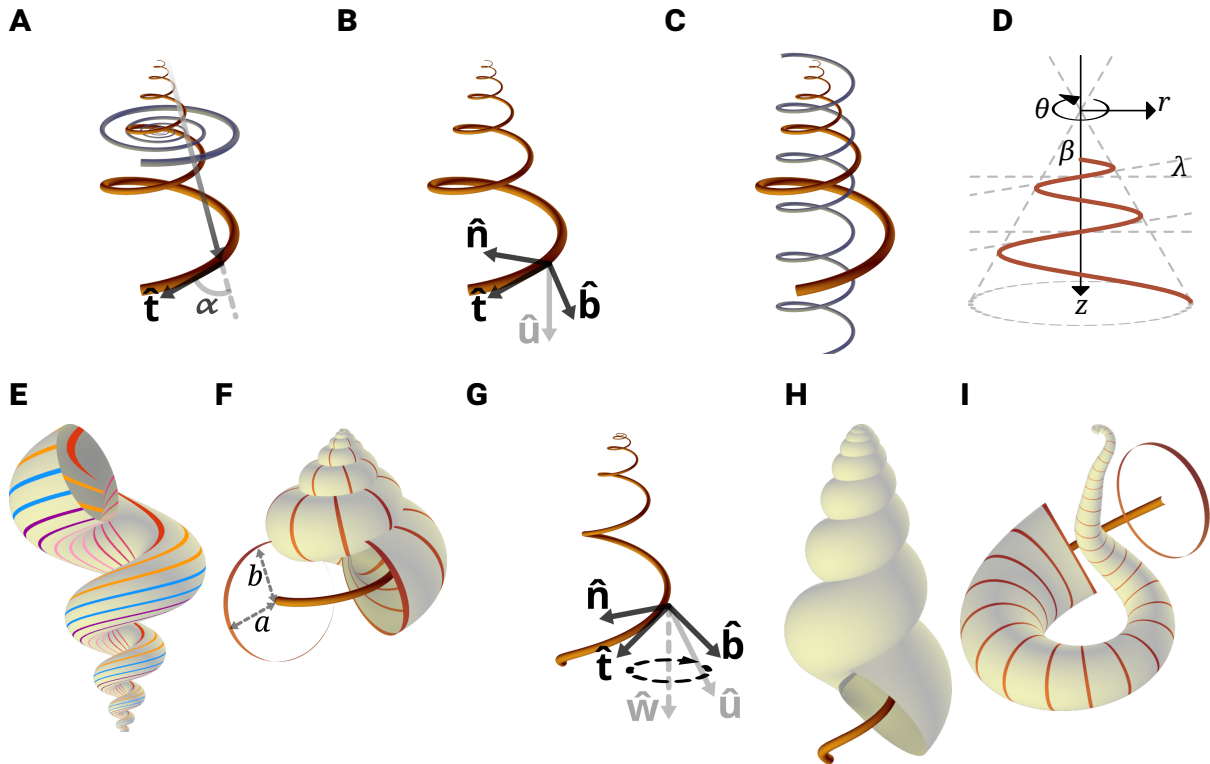
392 Tursch B (1997). Spiral growth: The ‘Museum of all shells’ revisited. *J Molluscan Stud* 63: 547–554.
393 <https://doi.org/10.1093/mollus/63.4.547>.

394 Urdy S, Goudemand N, Bucher H, Chirat R (2010). Allometries and the morphogenesis of the
395 molluscan shell: a quantitative and theoretical model. *J Exp Zool* 314B: 280–302.
396 [10.1002/jez.b.21337](https://doi.org/10.1002/jez.b.21337).

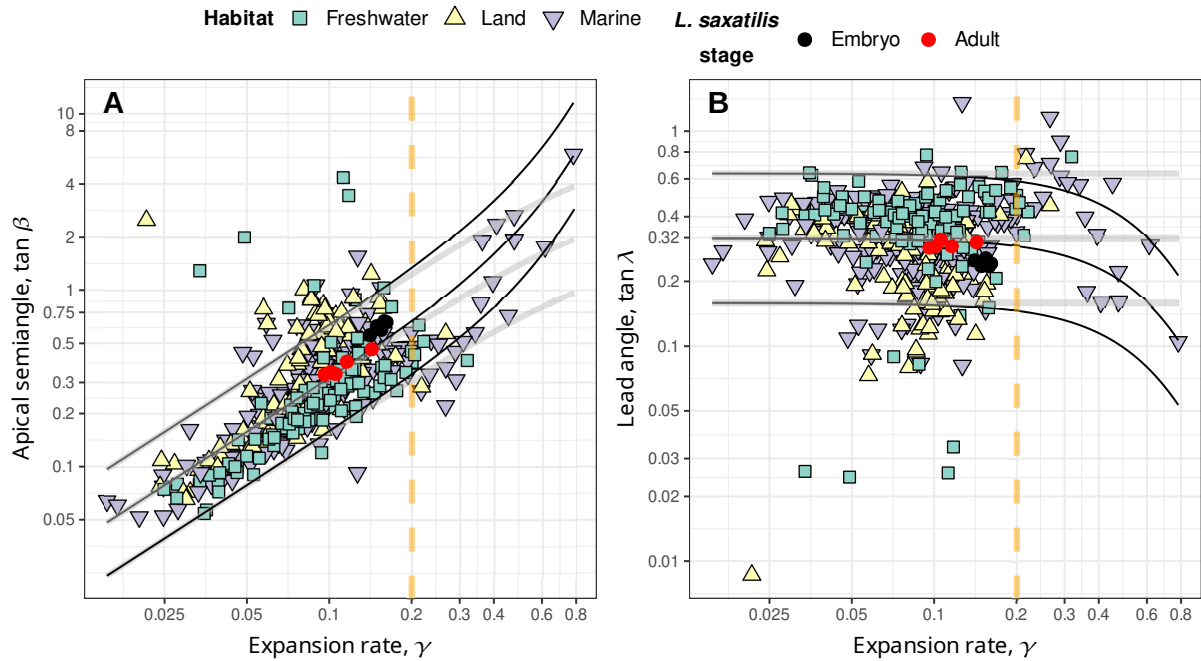
397 Uzunoğlu B, Gök I, Yaylı Y (2016). A new approach on curves of constant precession. *Applied*
398 *Mathematics and Computation* 275: 317–323. <https://doi.org/10.1016/j.amc.2015.11.083>.

399 van Osselaer C, Grosjean P (2000). Suture and location of the coiling axis in gastropod shells.

- 400 *Paleobiology* 26: 238–257. [10.1666/0094-8373\(2000\)026<0238:SAL0TC>2.0.CO;2](https://doi.org/10.1666/0094-8373(2000)026<0238:SAL0TC>2.0.CO;2).
- 401 Vermeij GJ (1993). *A Natural History of Shells*. Princeton University Press, Princeton, Oxford.
- 402 Vermeij GJ (2002). Characters in context: molluscan shells and the forces that mold them.
- 403 *Paleobiology* 28: 41–54. [10.1666/0094-8373\(2002\)028<0041:CICMSA>2.0.CO;2](https://doi.org/10.1666/0094-8373(2002)028<0041:CICMSA>2.0.CO;2).
- 404 Vinarski MV (2014). The birth of malacology. when and how? *Zoosystematics and Evolution* 90: 1–5.
- 405 [10.3897/zse.90.7008](https://doi.org/10.3897/zse.90.7008).



406 Figure 1 : Theoretical morphology in a snailshell. (A,B,C) Three parameterizations of conical logspi-
 407 rals; respectively conispiral, differential geometric, and conihelical. (A) Constant spiral angle, α , between
 408 instantaneous tangent vector, $\hat{\mathbf{t}}$, and radius-vector from pole (apex) defines the conispiral parameteriza-
 409 tion. The conispiral is as if a corresponding logarithmic base planispiral (in blue), with same expansion
 410 rate, γ , has been stretched out of its plane, to form a three-dimensional space curve. (B) The differ-
 411 ential geometric parameterization follows the evolution of the Frenet moving frame, defined by tangent, $\hat{\mathbf{t}}$,
 412 principal normal, $\hat{\mathbf{n}}$, and binormal, $\hat{\mathbf{b}} = \hat{\mathbf{t}} \times \hat{\mathbf{n}}$. The frame's rotation is defined by the Darboux vector $\mathbf{u} = u \hat{\mathbf{u}} =$
 413 $\tau \hat{\mathbf{t}} + \kappa \hat{\mathbf{b}} = u \sin \lambda \hat{\mathbf{t}} + u \cos \lambda \hat{\mathbf{b}}$; κ is curvature, and τ torsion (SI). (C) In the conihelical parameterization, a conic-
 414 al logspiral is viewed as a helix with expanding radius – a conical helix. For comparison, a circular helix
 415 with same slope (i.e., lead angle) is also illustrated. (D) Conical helix in side view. Apical semiangle, β ,
 416 lead angle, λ , and the cylindrical coordinate system illustrated. The z -direction coincides with the coiling
 417 axis. (E) Multispiral approach to shell modeling, where shell surface is defined by many spiral paths, dif-
 418 fering in lead angle. For illustration purposes, an exaggerated open-coiled shell is shown, where slopes of
 419 inner spirals are clearly steeper. Nevertheless, all spirals share the same expansion rate, γ . (F) Generat-
 420 ing curve approach to shell modeling. Shell surface defined by a closed figure (here a circle) that sweeps
 421 along a conihelical centerline. Also illustrated are the size measures, a and b (not to be confused with the
 422 binormal vector, $\hat{\mathbf{b}}$), roughly corresponding respectively to aperture size perpendicular and parallel to the
 423 coiling axis. (G) In allometric shells, where centerline lead angle varies, the Darboux vector is no longer
 424 fixed, but rotates around an axis $\mathbf{w} = w \hat{\mathbf{w}}$ that contains a λ' component (Eq.[3]; SI). (H,I) Allometric and
 425 irregularly coiled shells with logarithmic slant helix centerline. Lead angles are initially 0 (i.e., planispiral
 426 coiling), but subsequently grow at different rates. Parameter values to simulate all shell images of this
 427 figure in the WebGL application are provided in SI.



429 Figure 2 : Apical semiangle, as $\tan \beta$ (panel A), and lead angle, as $\tan \lambda$ (panel B), against expansion
 430 rate, $\gamma = \ln W/2\pi$, from the data in Noshita *et al.* (2012) and Araki & Noshita (2023) on coiling parameters
 431 of over 400 species of freshwater, marine, and terrestrial gastropods, and the data of Newkirk & Doyle
 432 (1975) on embryos and adults of *Littorina saxatilis* from five different populations in Nova Scotia. In both
 433 panels, a vertical dashed line for $\gamma = 0.2$ marks roughly the domain of validity for small- γ approximations
 434 (SI), where nevertheless most data lies. Illustrated curves, however, were drawn using full (exact, non-
 435 approximate) expressions (SI). (A) When apical semiangle is plotted against expansion rate, a clear linear
 436 trend is visible. Solid black lines indicate boundaries for whorl-overlap, $\tan \beta > (1/\rho) \sinh(\pi\gamma)$, for $\rho =$
 437 0.5, 1, 2 (upper to lower; where ρ is defined as $\rho = b/a$, ratio of aperture sizes, as illustrated in Fig. 1F;
 438 $\rho = 1$ means a circular aperture) that separates tightly-coiled (above boundary line) and open-coiled shells
 439 (below boundary line). In the range $\gamma \leq 0.2$, such boundary curves for tight-coiling, however, are practically
 440 indistinguishable from relationships that fixed lead angles in Eq.[2] prescribe ($\tan \beta = (\gamma/\sqrt{1+\gamma^2}) \cot \lambda$;
 441 gray lines), given $\tan \lambda = \rho/\pi$ (SI; $D = 0$ for illustrated curves; i.e., apertures touching the coiling axis). Raw
 442 values for apical angles were transformed to correspond to centerlines by doubling reported values of
 443 T (see also, Davoli & Russo 1974). (B) Estimates of lead angle, $\tan \lambda$, obtained from Eq.[2]. Compared to
 444 panel A, there is clearly less variation in lead angle than in apical angle, and the linear trend disappears;
 445 suggesting independent variation in expansion rate, γ , and lead angle, λ . Black and gray solid curves
 446 correspond to those in panel A, but in reverse order ($\rho = 2, 1, 0.5$, upper to lower respectively).

428

447

S1 **Supplementary information for “Lead and slant on the geometry of coiling in**
S2 **gastropods”**

S3

S4 Ido Filin ¹ *

S5 ¹ Independent researcher.

S6 * Corresponding author. E-mail: ido@filin.fi

S7

S8 **Contents**

S9	S1 A note on terminology and notation	2
S10	S2 Expressions for logarithmic conispirals	3
S11	S3 Whorl-overlap condition for non-circular and displaced generating curves	4
S12	S4 Approximation errors	6
S13	S5 Differential geometric parameterization	6
S14	S6 Logarithmic slant helix	8
S15	S7 Web application	9
S16	S8 Supplementary references	10

S17 **S1 A note on terminology and notation**

S18 [Thompson \(\[1942\] 1992\)](#) defined three angles, related to the modeling of equiangular (i.e.,
S19 logarithmic) spiral shells. The spiral angle, α , is the angle between the radius-vector from the
S20 pole (or apex of the conical envelope) and the tangent to the spiral. His β denotes the apical
S21 semiangle, as in this study. His γ refers to the ‘angle of retardation’, relevant when considering
S22 the inner and outer margins of planispiral shells. Given that the angle of retardation has been
S23 rarely utilized since, I reclaim the symbol γ for denoting the exponential expansion rate in this
S24 study.

S25 Generalized or general helices ([Nutbourne & Martin 1988](#)) are defined by the constant slope,
S26 relative to a fixed direction. Hence, the alternative term, curve of constant slope ([Scofield](#)
S27 [1995](#)). Somewhat confusingly they are also often called ‘cylindrical helices’ ([O’Neill 2006](#)),
S28 referring to a generalized cylinder. But I avoid this term here.

S29 While ‘pitch’ is used often with circular helices to refer to the slope of the helix (e.g.,
S30 [Chouaieb et al. 2006](#)), strictly speaking, pitch is the distance between adjacent threads or
S31 strands. Lead, on the other hand, is the axial progression per one full revolution of the helical
S32 structure, which is the quantity of interest in this study. Lead and pitch are the same for
S33 single-thread helices, but not for double or triple helices, such as in double- and multi-start
S34 screws and various helical structures in biology.

S35 The slope of the helix, $\tan \lambda$, can be measured by the lead angle, as in this study, by the ‘helix
S36 slope’ itself (e.g., [De Renzi & Mayoral 2024](#); also ‘rise’, [Hauser et al. 2017](#)), or by the ‘helix
S37 angle’, relative to the fixed axis (the complementary angle to the lead angle; [Nutbourne &](#)
S38 [Martin 1988](#)). The latter was referred to as ‘inclination angle’ by [Moseley \(1842\)](#), in his work on
S39 conchylometry. However, more recently, inclination angle is used to describe the orientation
S40 of the aperture itself relative to the coiling axis ([Schindel 1990](#); [Vermeij 1993](#); [Noshita et al.](#)
S41 [2012](#)), so I avoid this term here.

S42 Finally, the quantity $u = \sqrt{\kappa^2 + \tau^2}$, which is the norm of the Darboux vector, where κ is
S43 curvature and τ is torsion, does not have a standard name. [Nutbourne & Martin \(1988\)](#) refer to
S44 it as ‘compound curvature’, and [Güzelkardeşler & Şahiner \(2024\)](#) call it ‘first alternative
S45 curvatrue’. Other appropriate terms may be ‘winding’, ‘writhe’, or ‘twist’, in reference to circular
S46 helices ([Chouaieb et al. 2006](#); [Goriely 2017](#)); but those usually involve additional meaning in
S47 terms of mechanical properties. It is also sometimes called angular rate, speed, or velocity,
S48 though time is only implicit here, and u measures rotation angle per unit arclength, not time.

s49 By the same token, the use of the term ‘spin’ is rejected. In this study, I refer to the Darboux
s50 vector and its norm, as well as to \mathbf{w} and w , simply as vectors and rates of coiling, as in the end,
s51 they describe direction and rate of rotation. While the greek letter ω is often used to denote
s52 the Darboux vector and $\sqrt{\kappa^2 + \tau^2}$ (Nutbourne & Martin 1988), I avoid this notation, so not to
s53 confuse with true angular velocity in mechanics.

s54 **S2 Expressions for logarithmic conispirals**

s55 Eq.[1] of the main text, $\cot \alpha \sin \beta = \gamma$, has been derived and used enough times, so not to require
s56 any explanation (Moseley 1842; Thompson [1942] 1992; Raup & Graus 1972; Løvtrup & von
s57 Sydow 1974; Ekaratne & Crisp 1983; Illert 1983). From geometry of cones, it is easy to see that

$$s58 \quad \sin \lambda = \cos \alpha \cos \beta \quad (S1)$$

s59 (Moseley 1842; up to differences in notation and definition of lead angle), the expression for
s60 spiral height dilation, q_z . These two equations can be combined to produce

$$s61 \quad \tan \lambda \tan \beta = \frac{\gamma}{\sqrt{1 + \gamma^2}}. \quad (S2)$$

s62 Values of γ for gastropods are typically below 0.2 (Thompson [1942] 1992; Cameron 1981;
s63 Fig. 3), corresponding to relatively slower expansion and shells that exhibit several complete
s64 whorls. For small values of γ , Eq.[S2] is approximated by Eq.[2] of the main text.

s65 The expression for a conispiral shell’s height-to-arclength ratio, derived by Ekaratne & Crisp
s66 (1983), can be written as $(z + b)/s$ in this study, which translates to $q_z + q_b = \sin \lambda + q_b$.

s67 Alternatively, using the steps of their derivation and following the suture spiral on the outer
s68 surface of the shell, rather than the centerline spiral, $(z/W + 2b)/s = (1/W) \sin \lambda + (2\rho a/s) =$

s69 $(1/W) \sin \lambda + \rho r/s = \sin \lambda (1/W + \rho \tan \beta)$ (where s , r , λ and β all refer now to the suture spiral, W
s70 is the whorl expansion rate [Eq.[S3] below], and using the relations $\rho = b/a$, $r = 2a$, and

s71 $r = z \tan \beta = s \sin \lambda \tan \beta$). In any case, all these ratios are constants for self-similar logarithmic
s72 conispiral shells.

S73 **S3 Whorl-overlap condition for non-circular and displaced generating curves**

S74 Mathematical and computational shell modeling got a boost with the work of David Raup in
S75 the 1960s (Raup 1961; Raup & Michelson 1965; Raup 1966) that also kick-started theoretical
S76 morphology. Raup's model for gastropod shell coiling (Raup 1961, 1966; Raup & Michelson
S77 1965) contains four parameters that are designed to be estimated from sagittal
S78 cross-sections of shells. His whorl expansion rate, W , is related to γ through

S79
$$W = e^{2\pi\gamma}. \quad (S3)$$

S80 His translation rate, T , is related to β by

S81
$$T = \cot \beta. \quad (S4)$$

S82 The *displacement* parameter (Schindel 1990), D , measures relative distance of the aperture
S83 from the coiling axis, and is given by

S84
$$D = \frac{r - a}{r + a}, \quad (S5)$$

S85 where a is aperture size in the radial direction (i.e., half the aperture's width in the r -direction).

S86 The umbilicus (or columellar) radius, ξ , i.e., distance of innermost aperture margin to the
S87 coiling axis, and the aperture size, a , are then given by

S88
$$\begin{aligned} a &= \left(\frac{1-D}{1+D}\right) r, \\ \xi &= r - a = \left(\frac{2D}{1+D}\right) r. \end{aligned} \quad (S6)$$

S89 Raup's fourth parameter, S , broadly refers to the shape of the generating curve, and is never
S90 really defined in his formulation. In principle, it may be vector- or function-valued, e.g., $S = S(\varphi)$
S91 (φ being some parameterization of the generating curve). It is, however, very often taken to be
S92 some ratio of major and minor axes of an ellipse — a natural extension of the circular
S93 generating curve (Raup 1966; Kohn & Riggs 1975; Newkirk & Doyle 1975; McNair *et al.* 1981;
S94 Ekaratne & Crisp 1983; Kemp & Bertness 1984; Ackerly 1992; Stone 1995; McGhee 1999; Clarke
S95 *et al.* 1999; Urdy *et al.* 2010; Larsson *et al.* 2020). Here, I follow Ekaratne & Crisp (1983) and
S96 define aperture size a , perpendicular to the coiling axis, and aperture size b , parallel to the
S97 axis, as illustrated in Fig. 1F of main text.

S98 The centers of two successive whorls (separated by $\Delta\theta = 2\pi$) are at distances r and rW
S99 from the coiling axis. Their distances to the apex are $r\sqrt{1+T^2}$ and $rW\sqrt{1+T^2}$, respectively.
S100 Aperture sizes along the conical envelope of the centerline spiral, i.e., at angle β to the coiling
S101 axis, are given by the radii of the elliptic generating curves at that angle $\frac{\rho a}{\sqrt{\rho^2 \sin^2 \beta + \cos^2 \beta}}$ and

S102 $\frac{\rho a W}{\sqrt{\rho^2 \sin^2 \beta + \cos^2 \beta}}$ respectively, where $\rho = b/a$. The whorl overlap condition is therefore,

$$S103 \quad r(W-1)\sqrt{1+T^2} < \frac{a\rho(W+1)\sqrt{1+T^2}}{\sqrt{\rho^2+T^2}}. \quad (S7)$$

S104 (recall that $T = \cot \beta$, and so $\sin^2 \beta = \frac{1}{1+T^2}$ and $\cos^2 \beta = \frac{T^2}{1+T^2}$). Substituting the expression for a
S105 from Eq.[S6], and further trivial manipulations give

$$S106 \quad T^2 < \rho^2 \left(\frac{\left(\frac{1-D}{1+D}\right)^2 (W+1)^2 - (W-1)^2}{(W-1)^2} \right), \quad (S8)$$

S107 or

$$S108 \quad T^2 < \rho^2 \frac{4W + 4D^2W - 4DW^2 - 4D}{(1+D)^2(W-1)^2}. \quad (S9)$$

S109 Substituting circular apertures ($\rho = 1$) in Eq.[S8] results in [Rex & Boss's \(1976\)](#) expression for
S110 the boundary between whorl-overlap and open coiling. For a circular aperture ($\rho = 1$) touching
S111 the coiling axis ($D = 0$), I obtain [Raup's \(1966\)](#) expression for the "univalve-bivalve" boundary,
S112 $T = \frac{2\sqrt{W}}{W-1}$, on the W - T face of his morphospace cube. Substituting $T = 0$ in Eq.[S7] gives the
S113 "univalve-bivalve" boundary on the W - D face, $D < 1/W$, which is [Raup's \(1966\)](#) whorl-overlap
S114 condition for planispiral shells.

S115 In terms of γ and β , Eq.[S8] can be rewritten as

$$S116 \quad \cot^2 \beta < \rho^2 \left(\left(\frac{1-D}{1+D} \right)^2 \coth^2(\pi\gamma) - 1 \right) = \rho^2 \left(\left(\frac{1-D}{1+D} \right)^2 \frac{1}{\sinh^2(\pi\gamma)} - \frac{4D}{(1+D)^2} \right) \quad (S10)$$

S117 or

$$S118 \quad \tan \beta > \frac{1+D}{\rho} \frac{\sinh(\pi\gamma)}{\sqrt{(1-D)^2 - 4D \sinh^2(\pi\gamma)}}. \quad (S11)$$

S119 For circular apertures ($a = b$; $\rho = 1$) and $D = 0$, this equation gives the expression of Raup's
S120 whorl-overlap boundary in terms of γ and β of this study, $\tan \beta = \sinh(\pi\gamma)$.

S121 From Eq.[S10] one can get the condition for whorl-overlap in terms of $\sin \beta$,

$$S122 \quad \sin^2 \beta > \frac{1}{\rho^2 \left(\frac{1-D}{1+D} \right)^2 \coth^2(\pi\gamma) + (1-\rho^2)}. \quad (S12)$$

S123 For $D = 0$ this simplifies to

$$S124 \quad \sin^2 \beta > \frac{\sinh^2(\pi\gamma)}{\sinh^2(\pi\gamma) + \rho^2}. \quad (S13)$$

S125 For $D = 0$ and $\rho = 1$, the condition further reduces to $\sin \beta > \tanh \pi\gamma$, the expression arrived at by
S126 [Clarke et al. \(1999\)](#); after correcting their typo and accounting for difference in definition of
S127 apical semiangle).

S128 Combining Eq.[S11] and Eq.[S2], I get the whorl-overlap boundary in terms of lead angle,

$$S129 \quad \tan \lambda < \frac{\rho}{1+D} \frac{\gamma \sqrt{(1-D)^2 - 4D \sinh^2(\pi\gamma)}}{\sqrt{1+\gamma^2} \sinh(\pi\gamma)}. \quad (S14)$$

S130 Applying the small- γ approximation, the whorl overlap condition for lead angle becomes

$$S131 \quad \tan \lambda < \left(\frac{1-D}{1+D} \right) \frac{\rho}{\pi} + \mathcal{O}(\gamma^2), \quad (S15)$$

S132 providing the corresponding fixed value of lead angle that matches the whorl overlap
S133 condition for particular aperture shape, ρ , and aperture displacement, D .

S134 **S4 Approximation errors**

S135 For the range of γ -values exhibited by most gastropods, $\gamma \leq 0.2$ (Thompson [1942] 1992;
S136 Cameron 1981), the error between the full and approximate versions of Eq.[S2] (Eq.[2] in the
S137 main text) is no more than 2%. This is derived from the ratio of the right-hand-sides of Eq.[2]
S138 and Eq.[S2], $\sqrt{1+\gamma^2}$, which clearly increases with γ , and is 1 for $\gamma=0$ and 1.0198 for $\gamma=0.2$.

S139 **S5 Differential geometric parameterization**

S140 The typical approach in differential geometry is to follow the Frenet frame, attached to a space
S141 curve; though other local (moving) frames are possible (Moulton & Goriely 2012; Moulton *et al.*
S142 2012; Uzunoğlu *et al.* 2016; Goriely 2017; Güzelkardeşler & Şahiner 2024 ; see below). The
S143 Frenet frame is composed of the tangent, principal normal, and binormal unit vectors of the
S144 space curve, $\hat{\mathbf{t}}$, $\hat{\mathbf{n}}$, and $\hat{\mathbf{b}}$, respectively, parameterized by arclength, s , along the curve. The frame
S145 changes along the curve according to the Frenet-Serret differential equations,

$$S146 \quad \begin{aligned} \hat{\mathbf{t}}' &= \frac{d\hat{\mathbf{t}}}{ds} = \mathbf{u} \times \hat{\mathbf{t}} = \kappa \hat{\mathbf{n}} \\ \hat{\mathbf{n}}' &= \mathbf{u} \times \hat{\mathbf{n}} = \tau \hat{\mathbf{b}} - \kappa \hat{\mathbf{t}} \\ \hat{\mathbf{b}}' &= \mathbf{u} \times \hat{\mathbf{b}} = -\tau \hat{\mathbf{n}}, \end{aligned} \quad (S16)$$

S147 where \times is vector cross-product in 3D Euclidean space, \mathbf{u} is the Darboux vector,

$$S148 \quad \mathbf{u} = u\hat{\mathbf{u}} = \tau\hat{\mathbf{t}} + \kappa\hat{\mathbf{b}}, \quad (S17)$$

S149 u is the vector's magnitude (i.e., local coiling; or the compound curvature of Nutbourne &
S150 Martin 1988; see §S1), $\kappa = u \cos \lambda$ is curvature, and $\tau = u \sin \lambda$ is torsion. The Darboux vector,
S151 thus, describes the instantaneous rotation of the Frenet moving-frame, with respect to
S152 arclength (rather than time). For generalized helices ($\tau/\kappa = \tan \lambda = \text{const}$), including conical
S153 helices, the direction of the Darboux vector is fixed, $\hat{\mathbf{u}}' = 0$, though coiling rate, u , itself can
S154 change (e.g., for conical helices $u \propto 1/s$). In other words, for generalized helices $\mathbf{u}' = u'\hat{\mathbf{u}}$, and
S155 the direction $\hat{\mathbf{u}}$ determines the fixed coiling axis of the helix.

S156 If lead angle changes with arclength, the space curve is no longer a generalized helix, and
S157 the direction of \mathbf{u} changes along the curve, $\hat{\mathbf{u}}' \neq 0$ and $\mathbf{u}' = u'\hat{\mathbf{u}} + u\hat{\mathbf{u}}'$. Because $\hat{\mathbf{u}}$ is a unit vector,

S158 its derivative can be written as a cross-product with some instantaneous rotation vector, \mathbf{w} ,
S159 such that $\hat{\mathbf{u}}' = \mathbf{w} \times \hat{\mathbf{u}}$. For generalized helices $\mathbf{w} \equiv \mathbf{u}$, and so $\hat{\mathbf{u}}' = \mathbf{u} \times \hat{\mathbf{u}} = u \hat{\mathbf{u}} \times \hat{\mathbf{u}} \equiv 0$. In the general
S160 case, we write $\mathbf{w} = w_1 \hat{\mathbf{t}} + w_2 \hat{\mathbf{n}} + w_3 \hat{\mathbf{b}}$, and attempt to find the w_i from Eqs.[S16] and [S17].

S161 First, note that from Eq.[S17] $\hat{\mathbf{u}} = \hat{\mathbf{t}} \sin \lambda + \hat{\mathbf{b}} \cos \lambda$, and therefore by applying the Frenet-Serret
S162 relations (Eq.[S16]), $\hat{\mathbf{u}}' = (\hat{\mathbf{t}} \cos \lambda - \hat{\mathbf{b}} \sin \lambda) \lambda'$. Expanding the rotation vector,
S163 $\mathbf{w} \times \hat{\mathbf{u}} = (-w_2 \hat{\mathbf{b}} + w_3 \hat{\mathbf{n}}) \sin \lambda + (-w_1 \hat{\mathbf{n}} + w_2 \hat{\mathbf{t}}) \cos \lambda$. Equating the two expressions per component,
S164 one obtains $w_2 = \lambda'$, and $w_3 = w_1 \cot \lambda$, while w_1 still remains unknown. We can already guess,
S165 based on $\mathbf{w} = \mathbf{u}$ for generalized helices, that $w_1 = u \sin \lambda = \tau$ and $w_3 = u \cos \lambda = \kappa$. That is
S166 corroborated by noting that the Darboux vector does not have a $\hat{\mathbf{n}}$ -component, i.e., $\hat{\mathbf{u}}$ and $\hat{\mathbf{n}}$ are
S167 always perpendicular to each other. Consequently, we can construct the alternative
S168 orthonormal moving-frame of [Uzunoğlu et al. \(2016\)](#) and [Güzelkardeşler & Şahiner \(2024\)](#),
S169 composed of $\hat{\mathbf{u}}$, $\hat{\mathbf{n}}$, and $\hat{\mathbf{u}} \times \hat{\mathbf{n}}$. The rotation vector of this frame is \mathbf{w} , resulting in the relation
S170 $\hat{\mathbf{n}}' = \mathbf{w} \times \hat{\mathbf{n}} = w_1 \hat{\mathbf{b}} - w_3 \hat{\mathbf{t}}$. But from the Frenet-Serret equations (Eq.[S16]) we know that $\hat{\mathbf{n}}' = \tau \hat{\mathbf{b}} - \kappa \hat{\mathbf{t}}$,
S171 and so $w_1 = \tau$ and $w_3 = \kappa$, or in vector form,

$$\begin{aligned} \mathbf{w} &= w \hat{\mathbf{w}} = \mathbf{u} + \lambda' \hat{\mathbf{n}} = u \hat{\mathbf{u}} + \lambda' \hat{\mathbf{n}}, \\ w &= \sqrt{u^2 + (\lambda')^2}, \end{aligned} \tag{S18}$$

S173 the vector and rate of total coiling, respectively. Comparing again to [Uzunoğlu et al. \(2016\)](#) and
S174 [Güzelkardeşler & Şahiner \(2024\)](#), u is their ‘first alternative curvature’, and λ' their ‘second
S175 alternative curvature’. Generalized helices are obtained when the second alternative curvature
S176 vanishes, $\lambda' = 0$ ([Güzelkardeşler & Şahiner 2024](#)). Substituting the identity $\tan \lambda = \kappa / \tau$ into their
S177 expression for the second alternative curvature, $\frac{\kappa^2}{\kappa^2 + \tau^2} (\kappa / \tau)'$, clearly results in $\cos^2 \lambda \, d \tan \lambda / ds$,
S178 which reduces to simply $d \lambda / ds \equiv \lambda'$. Namely, the second alternative curvature is simply the
S179 rate of change in lead angle, which I refer to as rate of *coiling precession*.

S180 For generalized helices ($\lambda = \text{const}$), $\mathbf{w} = \mathbf{u}$, $\hat{\mathbf{u}}' = \mathbf{w} \times \hat{\mathbf{u}} = -\lambda' (\hat{\mathbf{u}} \times \hat{\mathbf{n}}) = 0$, and there is a fixed
S181 coiling axis, coinciding with a fixed Darboux vector. However, in general, the vector \mathbf{w} defines a
S182 precession of the Darboux vector (recall that \mathbf{u} is the instantaneous rotation of the Frenet
S183 frame), and is itself not fixed. In some special cases, when $u = \text{const}$ and \mathbf{w} fixed, one can
S184 obtain the ‘modulated curves’ of [Nutbourne & Martin \(1988\)](#), better known as ‘curves of
S185 constant precession’ ([Scofield 1995](#)).

S186 A slant helix is, similarly, a class of precession curves that includes the generalized helix
S187 and the curves of constant precession as special cases. The defining feature of a slant helix
S188 is a constant angle between the principal normal of the curve, $\hat{\mathbf{n}}$, and some fixed direction in
S189 space. In generalized helices, that angle is 90° . [Izumiya & Takeuchi’s \(2004\)](#) necessary and

s190 sufficient condition for a slant helix translates, in the notation of this study, to the
s191 proportionality relationship $\lambda' = \sigma u$. In other words, second alternative curvature is
s192 proportional to first alternative curvature, with a proportionality constant σ . The total coiling
s193 vector becomes $\mathbf{w} = w\hat{\mathbf{w}} = u(\hat{\mathbf{u}} + \sigma\hat{\mathbf{n}})$, and $\hat{\mathbf{w}}$ defines a fixed axis of rotation (or coiling), though
s194 coiling rate, $w = u\sqrt{1 + \sigma^2}$, around the fixed axis generally varies. That can be verified by
s195 $\sqrt{1 + \sigma^2}\hat{\mathbf{w}}' = (\hat{\mathbf{u}} + \sigma\hat{\mathbf{n}})' = \mathbf{w} \times \hat{\mathbf{u}} + \sigma\mathbf{w} \times \hat{\mathbf{n}} = (\sigma u\hat{\mathbf{n}}) \times \hat{\mathbf{u}} + \sigma(u\hat{\mathbf{u}} \times \hat{\mathbf{n}}) = 0$.

s196 Finally, note that the lead angle, λ , is defined in the $\hat{\mathbf{t}}\hat{\mathbf{b}}$ plane, the *rectifying plane* of the space
s197 curve. For generalized helices, this plane is parallel to the coiling axis, i.e. z -axis, and lead
s198 angle therefore is the angle between $\hat{\mathbf{t}}$ and the r - θ (or x - y) plane, perpendicular to the coiling
s199 axis; or, alternatively, the z -component of $\hat{\mathbf{t}}$ is $\sin \lambda$. That is no longer the case for slant helices.
s200 The rectifying plane now revolves around the coiling axis at a fixed tilt, given by $\arctan(\sigma)$. Lead
s201 angle is still defined in the rectifying plane, and therefore the tangent vector, $\hat{\mathbf{t}}$, which is also the
s202 unit velocity vector of the space curve w.r.t to arclength, is given in Cartesian coordinates by

$$\hat{\mathbf{t}} = (-\cos \lambda \sin \theta + c \sin \lambda \cos \theta)\hat{\mathbf{x}} + (\cos \lambda \cos \theta + c \sin \lambda \sin \theta)\hat{\mathbf{y}} + \sqrt{1 - c^2} \sin \lambda \hat{\mathbf{z}}, \quad (\text{S19})$$

s203 where $c = \frac{\sigma}{\sqrt{1 + \sigma^2}} = \text{const}$,

s204 and $\lambda = \lambda(s)$, $\theta = \theta(s)$. The rotation of $\hat{\mathbf{t}}$ is still given by the Frenet-Serret relations (Eq.[S16]),
s205 which translates in the case of slant helices to $\hat{\mathbf{t}}' = (\mathbf{w} - \lambda'\hat{\mathbf{n}}) \times \hat{\mathbf{t}} = \mathbf{w} \times \hat{\mathbf{t}} - \lambda'\hat{\mathbf{n}} \times \hat{\mathbf{t}}$. In other words,
s206 as expected, a combination of rotation around the axis, $\hat{\mathbf{w}}$, and rotation within the $\hat{\mathbf{t}}\hat{\mathbf{b}}$ plane at
s207 an angular rate λ' , as lead angle increases (with the axis of the latter rotation being $-\hat{\mathbf{n}}$; again,
s208 as expected according to the definition of lead angle).

s209 S6 Logarithmic slant helix

s210 For the logarithmic slant helix, $u = \tilde{u}/s$. Consequently, $\lambda' = \sigma \tilde{u}/s$ and $w = \tilde{w}/s$, where
s211 $\tilde{w} = \tilde{u}\sqrt{1 + \sigma^2}$. Given that $d\theta/ds = w$, it is straightforward to get relations comparable to conical
s212 helices for revolution angle and arclength, $\theta = \tilde{w} \ln(s/s_0)$ and $s = s_0 e^{\gamma\theta}$, where $\gamma = 1/\tilde{w}$ (in this
s213 section, $\gamma \equiv \gamma_s$). Given $\lambda' = d\lambda/ds = \sigma u = c w = c d\theta/ds$ (c as in Eq.[S19]), lead angle increases
s214 linearly with revolution angle according to $\lambda = \lambda_0 + c\theta$. From these expressions one can obtain
s215 the position vector of the logarithmic slant helix, $x(\theta)\hat{\mathbf{x}} + y(\theta)\hat{\mathbf{y}} + z(\theta)\hat{\mathbf{z}}$, by integrating $(ds/d\theta)\hat{\mathbf{t}}(s)$
s216 w.r.t to θ , given Eq.[S19] for $\hat{\mathbf{t}}(s)$,

$$z(\theta) = C_z + \sqrt{1 - c^2} s_0 e^{\gamma\theta} \left(\frac{\gamma^2 \sin(c\theta + \lambda_0) - c\gamma \cos(c\theta + \lambda_0)}{c^2 + \gamma^2} \right), \quad (\text{S20})$$

s217

$$x(\theta) = C_x + \frac{\gamma s_0 e^{\gamma\theta}}{c^4 + 2c^2\gamma^2 - 2c^2 + \gamma^4 + 2\gamma^2 + 1} (-c^4 \cos \lambda \cos \theta + c^3 \gamma \sin \lambda \cos \theta - 2c^3 \sin \lambda \sin \theta - c^2 \gamma^2 \cos \lambda \cos \theta - 3c^2 \gamma \sin \theta \cos \lambda + c\gamma^3 \sin \lambda \cos \theta + 3c\gamma \sin \lambda \cos \theta + 2c \sin \lambda \sin \theta - \gamma^3 \sin \theta \cos \lambda + \gamma^2 \cos \lambda \cos \theta - \gamma \sin \theta \cos \lambda + \cos \lambda \cos \theta), \quad (\text{S21})$$

$$y(\theta) = C_y + \frac{\gamma s_0 e^{\gamma\theta}}{c^4 + 2c^2\gamma^2 - 2c^2 + \gamma^4 + 2\gamma^2 + 1} (-c^4 \sin \theta \cos \lambda + c^3 \gamma \sin \lambda \sin \theta + 2c^3 \sin \lambda \cos \theta - c^2 \gamma^2 \sin \theta \cos \lambda + 3c^2 \gamma \cos \lambda \cos \theta + c\gamma^3 \sin \lambda \sin \theta + 3c\gamma \sin \lambda \sin \theta - 2c \sin \lambda \cos \theta + \gamma^3 \cos \lambda \cos \theta + \gamma^2 \sin \theta \cos \lambda + \gamma \cos \lambda \cos \theta + \sin \theta \cos \lambda), \quad (\text{S22})$$

s218 where C_z , C_x , C_y are determined from initial conditions, and $\lambda = \lambda(\theta) = \lambda_0 + c\theta$. These
s219 expressions for $x(\theta)$, $y(\theta)$ and $z(\theta)$, can be used in computer graphics to simulate shells that
s220 follow a logarithmic slant helix centerline.

s221 **S7 Web application**

s222 For this study, I have also written a WebGL application to help with creating images of shells, as
s223 in Fig. 1. Snapshot of the code, coinciding with the publication of this report, is available at
s224 <https://doi.org/10.5281/zenodo.19895626>.

- s225 • WebApp options and parameters for Fig. 1A–C are Shell unchecked, Centerline spiral
s226 checked, Generating curve unchecked, and either Planispiral (panel A) or Circular helix
s227 (panel C) additionally selected. Pitch angle 69° , Roll angle 200° , $\lambda_0 = 0.22$, $\tilde{w} = 11.43$
s228 ($\gamma = 0.0875$), $\sigma = 0$.
- s229 • Parameters for Fig. 1E are Pitch angle 270° , Roll angle 64° , Shell and Multispirals checked,
s230 Generating curve unchecked. $\lambda_0 = 0.39$, $\tilde{w} = 9.38$ ($\gamma = 0.107$), $\sigma = 0$.
- s231 • For Fig. 1F, Pitch angle 70° , Roll angle 257° . Shell, Centerline spiral, and Generating curve
s232 checked. $\lambda_0 = 0.22$, $\tilde{w} = 11.43$ ($\gamma = 0.0875$), $\sigma = 0$.
- s233 • Parameters for Fig. 1G are Pitch angle 69° , Roll angle 300° , Shell deselected, Centerline
s234 spiral checked, Generating curve unchecked, $\lambda_0 = 0$, $\tilde{w} = 11.43$ ($\gamma = 0.0875$), $\sigma = 0.013$.
- s235 • Parameters for Fig. 1H are Pitch angle 69° , Roll angle 36° , Shell deselected, Centerline
s236 spiral checked, Generating curve unchecked, $\lambda_0 = 0$, $\tilde{w} = 18.99$ ($\gamma = 0.0527$), $\sigma = 0.01$.
- s237 • For Fig. 1I, Pitch angle 62° , Roll angle 152° , Shell, Centerline spiral, and Generating curve
s238 checked, $\lambda_0 = 0$, $\tilde{w} = 5.85$ ($\gamma = 0.171$), $\sigma = 0.21$.

S239 **S8 Supplementary references**

- S240 Ackerly SC (1992). The structure of ontogenetic variation in the shell of *Pecten*. *Palaeontology* 35:
S241 847–867.
- S242 Cameron RAD (1981). Functional aspects of shell geometry in some british land snails. *Biol J Linn Soc*
S243 16: 157–167. <https://doi.org/10.1111/j.1095-8312.1981.tb01648.x>.
- S244 Chouaieb N, Goriely A, Maddocks JH (2006). Helices. *Proc Natl Acad Sci USA* 103: 9398–9403.
S245 <https://doi.org/10.1073/pnas.0508370103>.
- S246 Clarke RK, Grahame J, Mill PJ (1999). Variation and constraint in the shells of two sibling species of
S247 intertidal rough periwinkles (Gastropoda: *Littorina* spp.). *J Zool* 247: 145–154.
S248 [10.1111/j.1469-7998.1999.tb00978.x](https://doi.org/10.1111/j.1469-7998.1999.tb00978.x).
- S249 De Renzi M, Mayoral E (2024). Understanding behaviour through theoretical morphology: the case of
S250 helical-shaped burrows. *J Iber Geol* 50: 549–566. <https://doi.org/10.1007/s41513-024-00249-7>.
- S251 Ekaratne SUK, Crisp DJ (1983). A geometric analysis of growth in gastropod shells, with particular
S252 reference to turbinate forms. *Journal of Marine Biology Association UK* 63: 777–797.
S253 [10.1017/S0025315400071216](https://doi.org/10.1017/S0025315400071216).
- S254 Goriely A (2017). *The Mathematics and Mechanics of Biological Growth*. Springer.
S255 <https://doi.org/10.1007/978-0-387-87710-5>.
- S256 Güzelkardeşler G, Şahiner B (2024). An alternative approach to find the position vector of a general
S257 helix. *Celal Bayar University Journal of Science* 20: 54–60. [10.18466/cbayarfbe.1479066](https://doi.org/10.18466/cbayarfbe.1479066).
- S258 Hauser K, He Y, Garcia-Diaz M, Simmerling C, Coutsiyas E (2017). Characterization of biomolecular
S259 helices and their complementarity using geometric analysis. *Journal of Chemical Information and*
S260 *Modeling* 57: 864–874. <https://doi.org/10.1021/acs.jcim.6b00721>.
- S261 Illert C (1983). The mathematics of gnomonic seashells. *Math Biosci* 63: 21–56.
S262 [10.1016/0025-5564\(83\)90049-4](https://doi.org/10.1016/0025-5564(83)90049-4).
- S263 Izumiya S, Takeuchi N (2004). New special curves and developable surfaces. *Turkish Journal of*
S264 *Mathematics* 28: 153–164. [10.14943/83700](https://doi.org/10.14943/83700).
- S265 Kemp P, Bertness MD (1984). Snail shape and growth rates: evidence for plastic shell allometry in
S266 *Littorina littorea*. *Proc Natl Acad Sci USA* 81: 811–813. <https://doi.org/10.1073/pnas.81.3.811>.
- S267 Kohn AJ, Riggs AC (1975). Morphometry of the *Conus* shell. *Syst Zool* 24: 346–359.
S268 [10.1093/sysbio/24.3.346](https://doi.org/10.1093/sysbio/24.3.346).
- S269 Larsson J, Westram AM, Bengmark S, Lundh T, Butlin RK, Butlin RK (2020). A developmentally

S270 descriptive method for quantifying shape in gastropod shells. *J R Soc Interface* 17.
S271 <http://dx.doi.org/10.1098/rsif.2019.0721>.

S272 Løvtrup S, von Sydow B (1974). D'Arcy Thompson's theorem and the shape of the molluscan shell.
S273 *Bull Math Biol* 36: 567–575. [10.1016/S0092-8240\(74\)80051-0](https://doi.org/10.1016/S0092-8240(74)80051-0).

S274 McGhee GR (1999). *Theoretical Morphology: The Concept and Its Applications*. Perspectives in Earth
S275 History and Paleobiology. Columbia University Press, New York.

S276 McNair C, Kier W, LaCroix P, Linsley R (1981). The functional significance of aperture form in
S277 gastropods. *Lethaia* 14: 63–70. [10.1111/j.1502-3931.1981.tb01076.x](https://doi.org/10.1111/j.1502-3931.1981.tb01076.x).

S278 Moseley H (1842). On conchylometry. *Lond Edinb Dubl Phil Mag* 21: 300–305.
S279 <https://doi.org/10.1080/14786444208621551>.

S280 Moulton D, Goriely A, Chirat R (2012). Mechanical growth and morphogenesis of seashells. *J Theor*
S281 *Biol* 311: 69–79. <https://doi.org/10.1016/j.jtbi.2012.07.009>.

S282 Moulton DE, Goriely A (2012). Surface growth kinematics via local curve evolution. *J Math Biol* 68:
S283 81–108. [10.1007/s00285-012-0625-7](https://doi.org/10.1007/s00285-012-0625-7).

S284 Newkirk GF, Doyle RW (1975). Genetic analysis of shell-shape variation in *Littorina saxatilis* on an
S285 environmental cline. *Mar Biol* 30: 227–237. [10.1007/BF00390745](https://doi.org/10.1007/BF00390745).

S286 Noshita K, Asami T, Ubukata T (2012). Functional constraints on coiling geometry and aperture
S287 inclination in gastropods. *Paleobiology* 38: 322–334. [10.1666/10060.1](https://doi.org/10.1666/10060.1).

S288 Nutbourne AW, Martin RR (1988). *Differential geometry applied to curve and surface design:*
S289 *Foundations*. Ellis Horwood, Chichester, England.

S290 O'Neill B (2006). *Elementary Differential Geometry*. Revised 2nd edn. Academic Press.

S291 Raup DM (1961). The geometry of coiling in gastropods. *Proc Natl Acad Sci USA* 47: 602–609.
S292 <https://doi.org/10.1073/pnas.47.4.602>.

S293 Raup DM (1966). Geometric analysis of shell coiling: general problems. *J Paleontol* 40: 1178–1190.

S294 Raup DM, Graus RR (1972). General equations for volume and surface area of a logarithmically coiled
S295 shell. *Mathematical Geology* 4: 307–316. [10.1007/BF02114092](https://doi.org/10.1007/BF02114092).

S296 Raup DM, Michelson A (1965). Theoretical morphology of the coiled shell. *Science* 147: 1294–1295.
S297 [10.1126/science.147.3663.1294](https://doi.org/10.1126/science.147.3663.1294).

S298 Rex MA, Boss KJ (1976). Open coiling in recent gastropods. *Malacologia* 15: 289–297.

S299 Schindel DE (1990). Unoccupied morphospace and the coiled geometry of gastropods: architectural
S300 constraint or geometric covariation? In *Causes of Evolution: a paleontological perspective* (edited by

- s301 Ross R, Allmon W), pp. 270–304. University of Chicago Press, Chicago.
- s302 Scofield PD (1995). Curves of constant precession. *The American Mathematical Monthly* 102: 531–537.
- s303 <https://doi.org/10.1080/00029890.1995.12004613>.
- s304 Stone JR (1995). CerioShell: a computer program designed to simulate variation in shell form.
- s305 *Paleobiology* 21: 509–519. [10.1017/S0094837300013518](https://doi.org/10.1017/S0094837300013518).
- s306 Thompson DW ([1942] 1992). *On Growth and Form: The Complete Revised Edition*. Dover, New York.
- s307 Urdy S, Goudemand N, Bucher H, Chirat R (2010). Allometries and the morphogenesis of the
- s308 molluscan shell: a quantitative and theoretical model. *J Exp Zool* 314B: 280–302.
- s309 [10.1002/jez.b.21337](https://doi.org/10.1002/jez.b.21337).
- s310 Uzunoğlu B, Gök I, Yaylı Y (2016). A new approach on curves of constant precession. *Applied*
- s311 *Mathematics and Computation* 275: 317–323. <https://doi.org/10.1016/j.amc.2015.11.083>.
- s312 Vermeij GJ (1993). *A Natural History of Shells*. Princeton University Press, Princeton, Oxford.